

Bounds on the fine structure constant variability from Fe II absorption lines in QSO spectra

Paolo Molaro^{1,a}, Dieter Reimers², Irina I. Agafonova³, and Sergei A. Levshakov³

¹ Osservatorio Astronomico di Trieste, Via G. B. Tiepolo 11, 34131 Trieste, Italy

² Hamburger Sternwarte, Universität Hamburg, Gojenbergsweg 112, D-21029 Hamburg, Germany

³ Ioffe Physico-Technical Institute, St. Petersburg, Russia

Abstract. The Single Ion Differential α Measurement (SIDAM) method for measuring $\Delta\alpha/\alpha$ and its figures of merit are illustrated together with the results produced by means of Fe II absorption lines of QSO intervening systems. The method provides $\Delta\alpha/\alpha = -0.12 \pm 1.79$ ppm (parts-per-million) at $z_{\text{abs}} = 1.15$ towards HE 0515-4414 and $\Delta\alpha/\alpha = 5.66 \pm 2.67$ ppm at $z_{\text{abs}} = 1.84$ towards Q 1101-264, which are so far the most accurate measurements for single systems. SIDAM analysis for 3 systems from the Chand et al. (2004) sample provides inconsistent results which we interpret as due to calibration errors of the Chand et al. data at the level ≈ 10 ppm. In one system evidence for photo-ionization Doppler shift between Mg II and Fe II lines is found. This evidence has important bearings on the Many Multiplet method where the signal for $\Delta\alpha/\alpha$ variability is carried mainly by systems involving Mg II absorbers. Some correlations are also found in the Murphy et al. sample which suggest larger errors than previously reported. Thus, we consider unlikely that both the Chand et al. and Murphy et al. datasets could provide an estimate of $\Delta\alpha/\alpha$ with an accuracy at the level of 1 ppm. A new spectrograph like the ESPRESSO project will be crucial to make progress in the astronomical determination of $\Delta\alpha/\alpha$.

1 Introduction

A hypothetical variability of the fine structure constant α has been widely discussed in the literature in the last few years for its great implications on fundamental physics (Dent, these proceedings) and cosmology (Avelino et al. 2006; Martins 2007, Fujii 2007).

Laboratory experiments are setting limits on any changes in α at low energy to 15 significant figures $|\dot{\alpha}/\alpha| = (-2.6 \pm 3.9) \times 10^{-16} \text{ yr}^{-1}$ (Peik et al. 2006) and an even lower limit is set by the fission product analysis of a natural reactor in Oklo at $1.2 \times 10^{-17} \text{ yr}^{-1}$ (Gould et al. 2006) occurred at redshift $z \simeq 0.2$. Being linearly extrapolated to higher redshifts ($z > 1$, $\Delta t \sim 10^{10}$ yr), the laboratory bound leads to $|\Delta\alpha/\alpha| \equiv |(\alpha_z - \alpha)/\alpha| < 5$ ppm (ppm stands for parts per million, 10^{-6}) and the Oklo limit leads to $|\Delta\alpha/\alpha| < 0.1$ ppm. However, the behavior of the $\Delta\alpha/\alpha$ variation can be more complex and several theories predict very different patterns ranging from slow-rolling to oscillating (e.g., Marciano 1984; Mota & Barrow 2004; Fujii 2005) and a linear extrapolation may not be valid on a cosmic time scale.

Variations of α at early cosmological epochs can be probed at very high redshift ($z \sim 10^{10}$) through the dependence of primordial light element abundances on fundamental parameters (e.g., Dent et al. 2007, Coc et al 2007) and at lower redshifts ($z \lesssim 6$) through the measurements of the relative radial velocity shifts between different metal absorption lines observed in quasar

^a e-mail: molaro@oats.inaf.it

Table 1. Atomic data and sensitivity coefficients Q for Fe II and Mg II lines

Line	$\lambda_{\text{vac}}^a, \text{\AA}$	f^b	Q_{old}^c	Q_{new}^d	$\Delta Q/Q$ (%)
Fe II	2600.1722	0.23878	0.035	0.0367	4^d
Fe II	2586.6494	0.06918	0.039	0.0398	3^d
Fe II	2382.7641	0.320	0.035	0.0369	4^d
Fe II	2374.4601	0.0313	0.038	0.0394	4^d
Fe II	2344.2128	0.114	0.028	0.0361	26^d
Fe II	1611.20034	0.00138	0.018	0.0251	32^d
Fe II	1608.45069	0.0580	-0.021	-0.0166	29^d
Mg II	2803.5315	0.3054	0.0034		8^a
Mg II	2796.3543	0.6123	0.0059		5^a

^aBased on MWF03, Aldenius et al. (2006), L07a.

^bOscillator strengths f are taken from Morton (2003).

^cDzuba et al. 1999, 2002. ^dPorsev et al. 2007.

spectra. Different transitions in molecules and atoms have different sensitivities to variations of the fundamental physical constants (Varshalovich & Levshakov 1993; Dzuba et al. 1999). This property leads to the Many Multiplet (MM) method (Webb et al. 1999; Murphy et al. 2006, hereafter MWF06). From the averaging over 143 absorption systems with redshifts $0.2 < z < 4.2$ identified in the Keck/HIRES spectra of more than one hundred of QSOs Murphy et al. (2004) obtained $\Delta\alpha/\alpha = -5.7 \pm 1.1$ ppm. Chand et al. (2004, hereafter CSPA) applying the MM method to 23 absorption systems from VLT/UVES spectra obtained $\Delta\alpha/\alpha = -0.6 \pm 0.6$ ppm. Observations of two individual systems by means of a slightly different methodology based only on Fe II lines, which will be described in some detail here, does not support variability of α as well (Levshakov 2004; Quast et al. 2004; Levshakov et al. 2005, 2006, 2007a, hereafter L07a). Thus, currently the case for variability is somewhat controversial with Murphy and collaborators claiming negative $\Delta\alpha/\alpha$ in the past at the level of ≈ -6 ppm at 5σ confidence level, and other groups insisting on non-variability of α at the ppm level.

2 The SIDAM method

2.1 Why only Fe II?

The spectroscopic measurability of $\Delta\alpha/\alpha$ is based on the fact that the energy of each line transition depends individually on a change in α . The relative change of the frequency ω_0 due to varying α is proportional to the so-called sensitivity coefficient $Q = q/\omega_0$. The q -factors for the resonance UV transitions were calculated by Dzuba et al. (2002). The updated values corrected for valence-valence and core-valence correlations and for the Breit interaction were recently reported by Porsev et al. (2007). Both the old and new sensitivity coefficients are listed in Table 1.

The value of $\Delta\alpha/\alpha$ itself depends on a proper interpretation of measured relative radial velocity shifts, Δv , between lines with different sensitivity coefficients. It can be shown (Levshakov et al. 2006, hereafter L06) that in linear approximation ($|\Delta\alpha/\alpha| \ll 1$)

$$\frac{\Delta\alpha}{\alpha} = \frac{(v_2 - v_1)}{2c(Q_1 - Q_2)} = \frac{\Delta v}{2c\Delta Q}. \quad (1)$$

To improve the accuracy of $\Delta\alpha/\alpha$ measurements we proposed a procedure referred to as the Single Ion Differential α Measurement (SIDAM) (Levshakov 2004; Levshakov et al. 2005), where the ion is Fe II. This approach offers some advantages with comparison of the MM method, namely:

1) It is more effective since the Fe II lines provide positive and negative shifts with a larger ΔQ . Comparing $\lambda 1608$ with $\lambda 2382$ or $\lambda 2600$ lines, we have $\Delta Q = -0.053$, which is almost

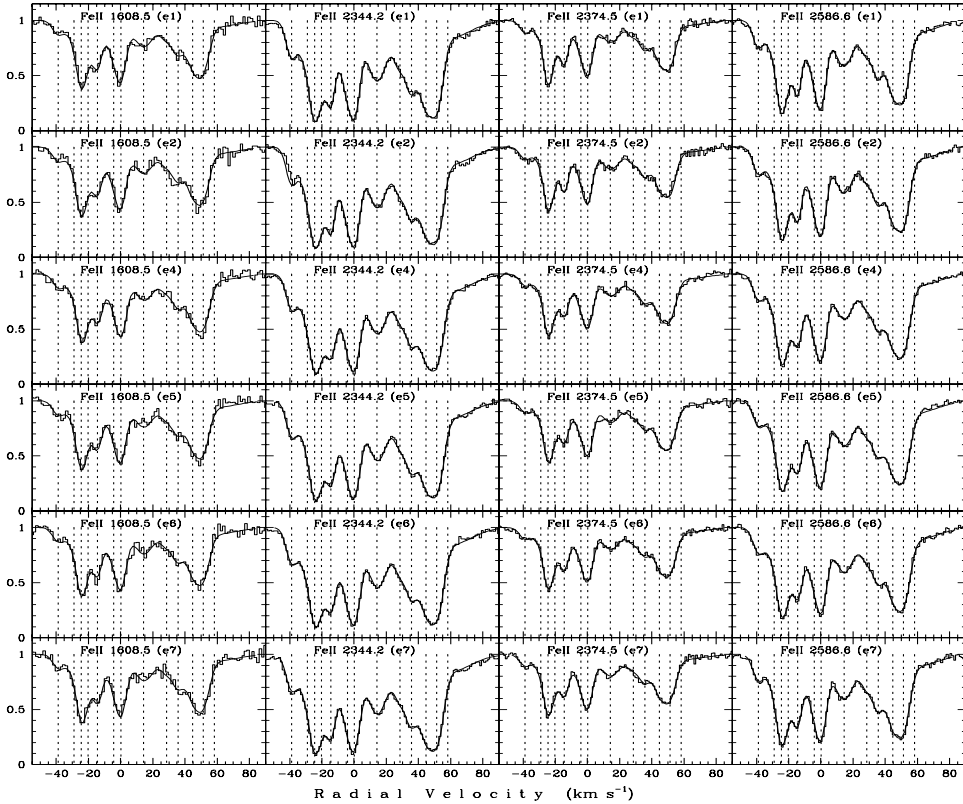


Fig. 1. Individual exposures of the Fe II lines of HE 0515–4414. Normalized intensities are histograms. The over-potted synthetic profiles (smooth curves) are calculated from the joint analysis of all Fe II profiles. The dashed vertical lines mark positions of the sub-components. The zero radial velocity is fixed at $z = 1.150965$. The minimization procedure gives $\chi^2_{\min} = 0.9$ per degree of freedom ($\nu = 2642$).

two times larger than the same quantity when one compares Mg II $\lambda\lambda 2796, 2803$ and Fe II $\lambda\lambda 2344, 2374, 2382, 2586, 2600$ transitions.

2) It is free from systematics inherent to inhomogeneous ionization. The MM method uses lines of different ions, which have different ionization curves. The fractional ionization of a given ion depends on the ionization parameter $U = n_{\text{ph}}/n_{\text{H}}$, where n_{ph} and n_{H} are, respectively, the density of the ionizing photons and the gas density. Hence, in a cloud with gas density fluctuations different ions are Doppler shifted with respect to each other (Levshakov 2004; Hao et al. 2007).

3) It is less sensitive to unknown isotopic abundances. The isotope shift between $^{26,24}\text{Mg}$ II transitions $3s \rightarrow 3p_{1/2}, 3p_{3/2}$ is $\Delta v_{24-26} \simeq 850 \text{ m s}^{-1}$. If the isotope abundance ratio indeed varies with z , the isotope shifts may imitate the non-zero $\Delta\alpha/\alpha$ value (Levshakov 1994; Ashenfelter et al. 2004; Kozlov et al. 2004). At metallicities of $Z \sim (0.1 - 1) Z_{\odot}$, — typical for the QSO systems with low ions, — the isotope abundances may not differ considerably from terrestrial. Unfortunately, we do not know the isotope abundances at different redshifts. The influence of unknown isotopic ratio can be considerably diminished if only Fe II is used. The isotopic effect for Fe II with seven valence electrons in the configurations $3d^6 4p$ and $3d^5 4s 4p$ is less pronounced than that for Mg II with only one valence electron in the configuration $3s$, because (i) iron is heavier and its isotope structure is more compact, and (ii) the relative abundance of the leading isotope ^{56}Fe is higher than that of ^{24}Mg . In fact the terrestrial isotope ratios for Fe are: $^{54}\text{Fe} : ^{56}\text{Fe} : ^{57}\text{Fe} : ^{58}\text{Fe} = 5.8 : 91.8 : 2.1 : 0.3$, while those for Mg are $^{24}\text{Mg} : ^{25}\text{Mg} : ^{26}\text{Mg} = 79 : 10 : 11$.

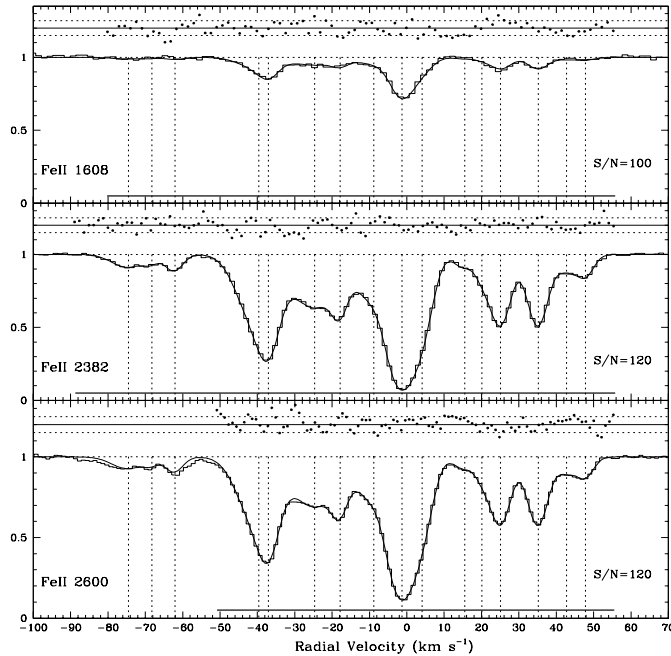


Fig. 2. Combined absorption-line spectra of Fe II associated with the $z_{\text{abs}} = 1.84$ damped Ly α system towards Q 1101–264 (normalized intensities are shown by histograms). The zero radial velocity is arbitrarily fixed at $z = 1.838911$. The synthetic profiles are over-plotted by the smooth curves and the dotted vertical lines mark positions of the sub-components. The normalized residuals, $(\mathcal{F}_i^{\text{cal}} - \mathcal{F}_i^{\text{obs}})/\sigma_i$, are shown by dots with the 1σ band by dotted lines. Bold horizontal lines mark pixels included in the optimization procedure. The ranges at $v < -50 \text{ km s}^{-1}$ and at $v \simeq -30 \text{ km s}^{-1}$ in the Fe II $\lambda 2600$ profile are blended with weak telluric lines. The normalized $\chi^2_\nu = 0.901$ ($\nu = 257$).

4) Less model dependent. All Fe II transitions used in SIDAM have identical velocity structure what helps to distinguish the influence of hidden blends on the line position measurements.

We have applied the SIDAM methodology only to the brightest QSO which provide a better control of instrumental and data reduction systematics. When possible we analyze single observations, which allow us to follow all individual steps of spectral recording. For instance calibration exposures should be taken immediately after scientific exposures to minimize the influence of changing ambient weather conditions which may cause different velocity offsets in the lamp and QSO spectra if they were not obtained closely in time. Variations in temperature can induce color effects in the spectra since they act differently on the different cross disperses. To control possible systematics in radial velocities, the thermal and pressure stabilities need to be monitored. The estimations of Kaufer et al. (2004) for UVES are of 50 m s^{-1} for $\Delta T = 0.3 \text{ K}$ and $\Delta P = 1 \text{ mbar}$.

Using SIDAM, we have almost reached the accuracy of $\Delta\alpha/\alpha$ of $\sim 10^{-6}$ for one absorption system, i.e. as high as the accuracy of the mentioned above values formally obtained from averaging over many absorption systems where individual $\Delta\alpha/\alpha$ values were measured with a considerably larger than 1 ppm error (see, e.g., Table 3 below).

2.2 Results

2.2.1 $\Delta\alpha/\alpha$ at $z_{\text{abs}} = 1.15$ towards HE 0515–4414

The first application of the SIDAM method yielded $\Delta\alpha/\alpha = -0.4 \pm 1.9 \text{ ppm}$ at $z_{\text{abs}} = 1.15$ towards the $B = 15.0$ bright quasar HE 0515–4414 (Quast et al. 2004). This accuracy was

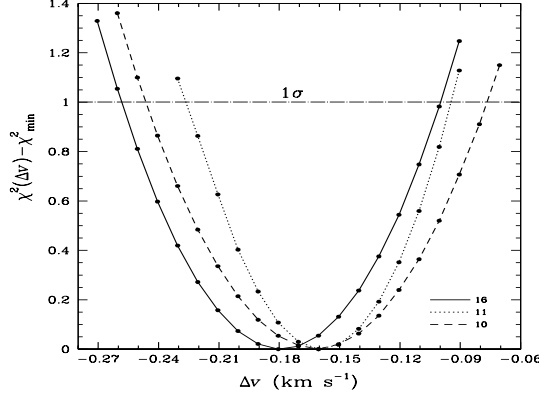


Fig. 3. The $z_{\text{abs}} = 1.84$ systems towards Q 1101–264: χ^2 as a function of the velocity difference Δv between the Fe II $\lambda 1608$ and $\lambda \lambda 2382, 2600$ lines for the 16-, 11-, and 10-component models. The corresponding χ^2_{\min} values are equal to 231.631, 135.314, and 166.397 (the number of degrees of freedom ν 257, 188, and 191, respectively). The minima of the curves give the most probable values of $\Delta\alpha/\alpha$: 5.4 ppm (the 16-component model) and 4.8 ppm (the 11- and 10-component models). The 1σ C.L. gives $\sigma_{\Delta v} = 0.080 \text{ km s}^{-1}$, 0.065 km s^{-1} , and 0.085 km s^{-1} or $\sigma_{\Delta\alpha/\alpha} = 2.4 \text{ ppm}$, 1.9 ppm , and 2.5 ppm for the 16-, 11-, and 10-component models, respectively

achieved due to unique favorable conditions such as the brightness of the quasar, high spectral resolution ($FWHM \simeq 5 \text{ km s}^{-1}$), and the strength of all Fe II lines including $\lambda 1608 \text{ \AA}$.

The system consists of two sub-systems with $z_1 = 1.151$ and $z_2 = 1.149$. The former reveals stronger Fe II lines and, hence, provides a higher accuracy of $\Delta\alpha/\alpha$. The 6 different spectra of this subsystem analyzed by L06 are reproduced in Fig. 1. L06 improved the accuracy of $\Delta\alpha/\alpha$ obtaining $\Delta\alpha/\alpha = -0.07 \pm 0.84 \text{ ppm}$, but this analysis did not take into account correlations between individual $\Delta\alpha/\alpha$ values (Levshakov et al. 2007b, hereafter L07b). If we consider k Fe II pairs with the radial velocity differences $a_1 = v_2 - v_1, a_2 = v_3 - v_1, \dots, a_k = v_{k+1} - v_1$, then the individual values a_i and a_j become correlated with the correlation coefficient $\rho_{i,j}$ given by

$$\rho_{i,j} = \frac{1}{\sqrt{(1 + s_i^2)(1 + s_j^2)}}, \quad (2)$$

where $s_i = \sigma_{v_i}/\sigma_{v_1}$, $s_j = \sigma_{v_j}/\sigma_{v_1}$, and v_1 stands for the radial velocity of the $\lambda 1608$ line. The errors of the line position measurements are almost equal for all lines. Thus the ratios in (2) are $s_i \simeq s_j \simeq 1$, i.e. in this case the correlation coefficient $\rho_{i,j} \simeq 0.5$. The error of the $\Delta\alpha/\alpha$ estimate from a pair of Fe II lines is equal to $\sigma_{\Delta\alpha/\alpha} \simeq 3.57 \text{ ppm}$, with the new Q values reported in Table 1. The calibration error is $\simeq 4 \text{ ppm}$ (L06) that gives the total $\sigma_{\Delta\alpha/\alpha} = 5.36 \text{ ppm}$. Considering that there are 18 pairs the error of the mean $\Delta\alpha/\alpha$ is 1.79 ppm (L07b) which is 2 times larger than the previous estimate. Thus, the revised value of $\Delta\alpha/\alpha$ at $z_{\text{abs}} = 1.15$ is $\Delta\alpha/\alpha = -0.12 \pm 1.79 \text{ ppm}$. This determination still remains the most accurate individual measurement obtained so far.

A consistent restriction on $\Delta\alpha/\alpha$ in this system was obtained independently by Chand et al. (2006), $\Delta\alpha/\alpha = 0.5 \pm 2.4 \text{ ppm}$, who used the high resolution pressure and temperature stabilized spectrograph HARPS mounted on the ESO 3.6 m telescope at the La Silla observatory. However, the calibration errors are not considered in the Chand et al. total error budget.

2.2.2 $\Delta\alpha/\alpha$ at $z_{\text{abs}} = 1.84$ towards Q 1101–264

The results on the system at $z_{\text{abs}} = 1.84$ towards Q 1101–264 are given in detail in L07a. The observations of Q 1101–264 were recorded with the VLT UV-Visual Echelle Spectrograph

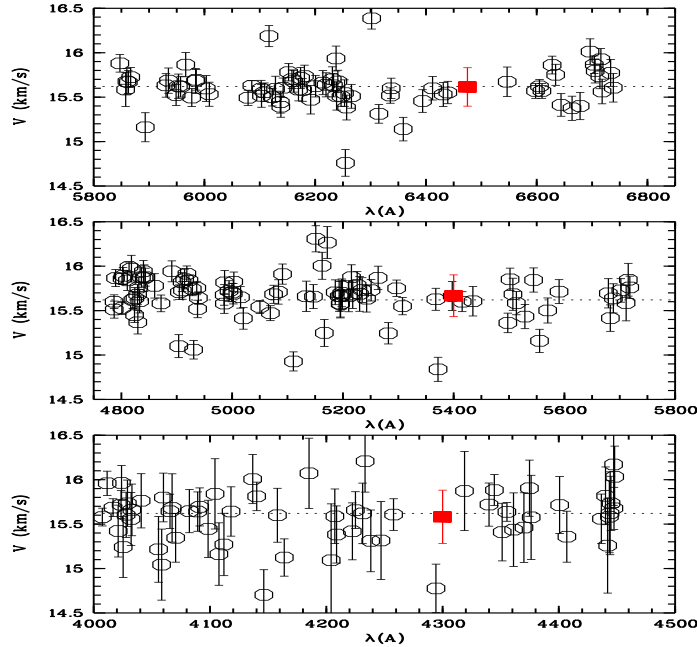


Fig. 4. Line shifts of Iris with reference of the solar line wavelengths (open circles with 1σ error bars). The dotted line shows the expected velocity of the asteroid. The panels refer to the three UVES CCDs. Mean values and their dispersion (solid squares with error bars) in the middle of each panel do not show any systematic shifts among them.

(UVES) on 3 nights in February 2006. The resulting normalized and co-added spectra from 9 exposures are shown in Fig. 2. A signal-to-noise ratio per pixel of $S/N \geq 100$ was achieved in the final spectrum. Particular care has been adopted in the observations. The 0.5 arcsec wide slit provided a spectral resolution of $FWHM \simeq 3.8 \text{ km s}^{-1}$ was oriented along the parallactic angle. Calibration exposures were taken immediately after scientific exposures allowing to minimize temperature and pressure changes. The pressure variation ΔP between the QSO exposure and the calibration lamp reached 0.6 mbar in one case, in all other cases did not exceed 0.3 mbar, while variations of the ambient temperature were always less than 0.1 K. The pixel sizes are of 25 mÅ, 30 mÅ and 27 mÅ at the positions of $\lambda 1608$, $\lambda 2382$ and $\lambda 2600$, respectively. The wavelength calibration was obtained from a ThAr hollow cathode lamp and the Los Alamos table of ThAr lines (Palmer & Engleman 1983; de Cuyper & Hensberge 1998) and the residuals of the calibrations were as small as about 20 m s^{-1} .

The Fe II lines selected for the analysis are those located close to the central regions of the corresponding echelle orders to minimize possible distortions of the line profiles caused by the decreasing spectral sensitivity at the edges of echelle orders. We found a good fit of Fe II profiles for a 16-component model shown in Fig. 2 by a smooth curve and the positions of the sub-components marked by dotted lines. The normalized χ^2 per degree of freedom equals $\chi^2_\nu = 0.901$ ($\nu = 257$). Since the Q values for $\lambda 2382$ and $\lambda 2600$ are equal, their relative velocity shift characterizes the goodness of our wavelength calibration. We measured a velocity shift of 20 m s^{-1} which is comparable with the uncertainty range estimated from the ThAr lines. So, we calculate the Δv between the velocity of these two lines and that of the $\lambda 1608$ line. To find the most probable value of Δv , we fit the absorption lines with a fixed Δv , changing Δv in the interval from -270 m s^{-1} to -90 m s^{-1} in steps of 10 m s^{-1} . For each Δv , the strengths of the sub-components, their broadening parameters and relative velocity positions were allowed to vary in order to optimize the fit and thus minimize χ^2 . The χ^2 curve as a function of Δv in the vicinity of the global minimum is shown in Fig. 3. The most probable value of Δv corresponds to -180 m s^{-1} for the 16-component model. The result is not sensitive

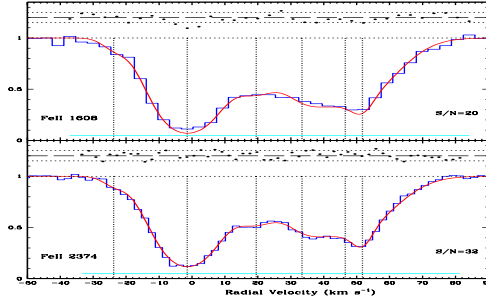


Fig. 5. The Fe II lines of the $z_{\text{abs}} = 1.776$ system towards QSO 1331+1704.

to the number of subcomponents in the model and we have also analyzed different models but showing similar radial velocity shifts between the $\lambda 1608$ and $\lambda 2383/2600$ lines. The 1σ errors are equal to 80 m s^{-1} , 65 m s^{-1} , and 85 m s^{-1} for the various models examined. Adding quadratically the wavelength scale calibration error of 30 m s^{-1} between the blue and red arms, L07a obtained $\Delta\alpha/\alpha = 5.4 \pm 2.5 \text{ ppm}$ for the main 16-component model. With the updated sensitivity coefficients Q_{new} the measurement in L07a becomes $\Delta\alpha/\alpha = 5.66 \pm 2.67 \text{ ppm}$.

This result is quite unexpected and in L07a we have specifically investigated those effects which might introduce a non-zero difference between the blue and the red lines and thus simulate a $\Delta\alpha/\alpha$ variation at the ppm level. Some systematics are discussed in L07a who were particularly concerned of the possibility that different velocity offsets occurring in the blue and red frames could cause an artificial Doppler shift between the $\lambda 1608$ and $\lambda 2382/2600$ lines. To probe this effect we developed a specific program of asteroid observations which are very high precision radial velocity standards. The results which are discussed in Molaro et al. (2007) and reproduced in Fig. 4 exclude that the shift observed is due to misalignment of the centering in the two slits of the arms of the UVES spectrograph.

2.2.3 The $z_{\text{abs}} = 1.776$ system towards QSO 1331+1704

The $z_{\text{abs}} = 1.776$ system towards QSO 1331+1704 is considered here for the first time for measuring $\Delta\alpha/\alpha$. The absorption system shows particularly strong lines with several metal lines saturated. This circumstance offers the unique opportunity to apply the analysis based on Fe II lines to two lines with comparable strength, namely the Fe II $\lambda 1608$ and $\lambda 2374$ shown in the Fig. 5. The crucial Fe II $\lambda 1608$ line is normally rather weak and is the bottleneck of the analysis. In this case the line is particularly strong making more effective the whole measure. We used two UVES archive images of 1 hour exposure taken on 18 and 23 Feb 2002. The analysis of the archive spectra is shown in Fig. 5 where the S/N is ≈ 20 -30. We have obtained a velocity difference of $\Delta v = -210 \pm 220 \text{ m s}^{-1}$, which implies $\Delta\alpha/\alpha = 5.9 \pm 6.2 \text{ ppm}$. This result is rather inconclusive due to the large error but obtained with very low S/N spectra. A relatively modest increase in the data quality will provide easily a much more accurate and significant measure of $\Delta\alpha/\alpha$.

3 SIDAM analysis of the Chand et al. sample

From the CSPA sample we selected few systems where the presence of several Fe II lines, including $\lambda 1608$, allowed us to estimate the value of $\Delta\alpha/\alpha$ with the SIDAM methodology. The three systems are $z_{\text{abs}} = 1.439$ towards HE 1347-2457, and $z_{\text{abs}} = 2.185$ and $z_{\text{abs}} = 2.187$ towards HE 0001-2340. These systems exhibit also a very simple line profiles which can be described by a minimum number of components thus minimizing the uncertainties related to model complex line profiles. In addition both the systems in HE 0001-2340 reveal unsaturated Mg II lines making it possible to compare the SIDAM $\Delta\alpha/\alpha$ value obtained with Fe II lines with that of the

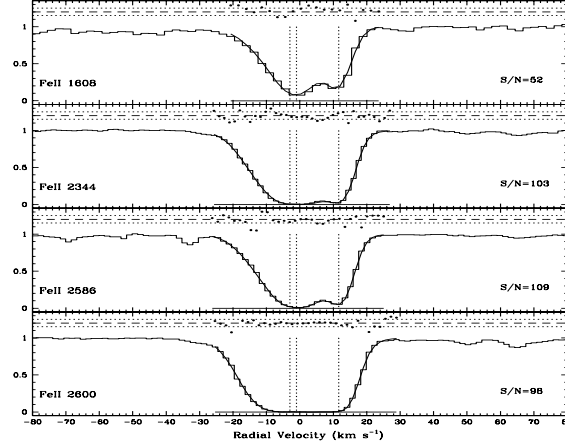


Fig. 6. Fe II lines of the $z_{\text{abs}} = 1.43925$ system towards HE 1347–2457. The model profiles are overplotted by the smooth curves. The normalized residuals, $(\mathcal{F}_i^{\text{cal}} - \mathcal{F}_i^{\text{obs}})/\sigma_i$, and 1σ errors are shown by dots. The vertical lines mark positions of the sub-components. Bold horizontal lines mark pixels included in the optimization procedure. The normalized $\chi^2_\nu = 1.43$ ($\nu = 109$).

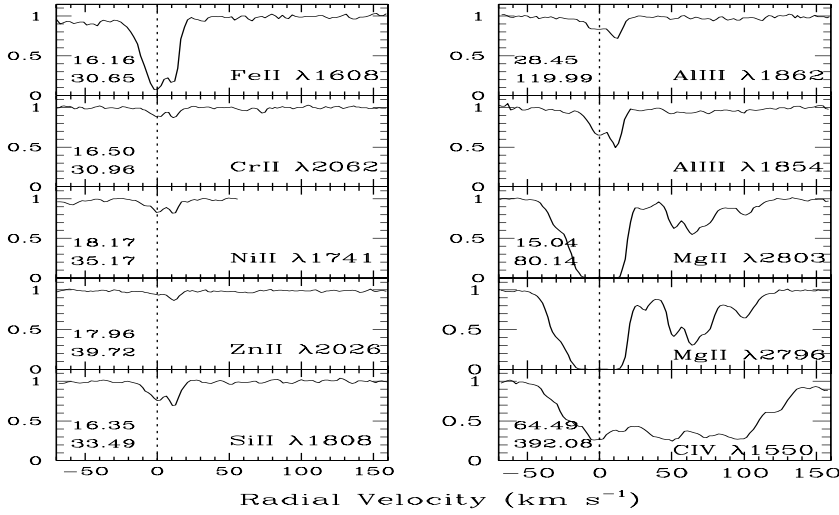


Fig. 7. Absorption lines associated with the $z_{\text{abs}} = 1.439$ system towards HE 1347–2457. The zero radial velocity is fixed at $z = 1.43925$. The ionization potentials (in eV) for the listed ions and their next ionization state are plotted in each panel. Note opposite asymmetry between subcomponents in Fe II, and Cr II, Ni II, Zn II, Si II, Al III in the range $-10 \leq v \leq 20 \text{ km s}^{-1}$. Besides, Mg II traces hotter gas seen also in Al III and C IV in the range $40 \leq v \leq 130 \text{ km s}^{-1}$.

MM method derived from the combination of Mg II and Fe II lines. For the analysis we used the reduced spectra courtesy provided by CSPA, but the continuum fitting was made by ourselves by means of the smoothing splines. We note that the data of CSPA were originally binned by 2×2 pixels, providing corresponding larger pixel sizes. A detailed analysis of these systems is presented in L07b.

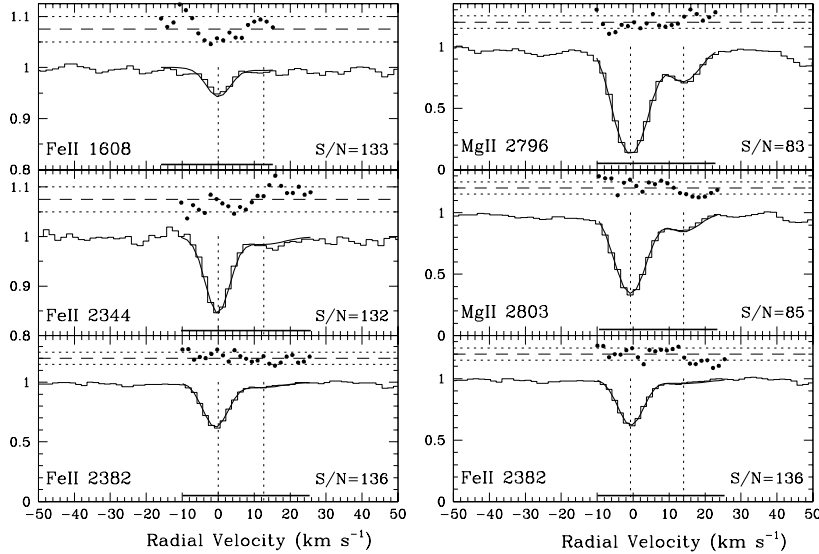


Fig. 8. Fe II and Mg I lines associated with the $z_{\text{abs}} = 2.185$ system towards HE 0001–2340. The zero radial velocity is fixed at $z = 2.1853$. The normalized χ^2_{ν} is equal to: 0.77 ($\nu = 57$) for the Fe II $\lambda\lambda 1608, 2344, 2382$ lines, and to 1.43 ($\nu = 54$) for the combined Mg I $\lambda\lambda 2796, 2803$ and Fe II $\lambda 2382$ lines. For other details see capture to Fig. 6.

3.1 HE 1347–2457

3.1.1 The $z_{\text{abs}} = 1.439$ system

The normalized spectra of four Fe II lines are shown in Fig. 7. The spectra have a rather high signal-to-noise ratio per pixel: $S/N = 52$, for the Fe II $\lambda 1608$, and ≈ 100 for the $\lambda 2344, \lambda 2586$, and $\lambda 2600$ lines. All Fe II lines were fitted simultaneously assuming identical velocity structure and allowing for the shift of this structure as a whole for every individual Fe II line. The corresponding synthetic line profiles for the three component model are shown by the smooth curves in Fig. 7.

The sensitivity coefficients of the *red* Fe II lines $\lambda\lambda 2344, 2586, 2600$ are very close to each other implying that for any $\Delta\alpha/\alpha$ value these lines should have the same relative radial velocity. Surprisingly, we found that the Fe II $\lambda 2600$ line shows a significant shift of $\sim -400 \text{ m s}^{-1}$ ($\sim 1/6$ pixel size) as compared to the Fe II $\lambda\lambda 2344, 2586$ lines. Considering that this line is close to the border of the echelle order where calibration errors may be large, we excluded it from the calculations.

From the velocity shift between the Fe II $\lambda 1608$ and the combined $\lambda\lambda 2344, 2586$ lines we estimate a $\Delta\alpha/\alpha = -21.3 \pm 2.1 \text{ ppm}$ (Q_{old} values from Table 1 are used here and in the following sub-sections in order to compare our calculations with the CSPA and MWF06 results). Taken at face value this result would provide a detection with a CL of 10σ . However, both the absolute value of $\Delta\alpha/\alpha$ and the significance level are very unlikely suggesting that the calibration errors are instead responsible for the observed shift. The accuracy of the above estimate characterizes solely the mutual consistency of the lines included in the χ^2 minimization, but do not consider the calibration errors. In the ESO archive we could not find calibration lamp exposures attached to the observations of HE 1347–2457 which means that the wavelength calibration was performed with lamps taken at a different moment. The large pixel size resulting from binning 2×2 pixels further deteriorates the accuracy. For instance, assuming a calibration error of $\sim 1/10$ pixel size, or uncertainties of $\sim 300 \text{ m s}^{-1}$ and $\sim 240 \text{ m s}^{-1}$ for the Fe II $\lambda 1608$ and Fe II $\lambda\lambda 2344, 2586$ lines, respectively, we get an error in $\Delta\alpha/\alpha$ of $\sigma_{\text{sys}} = 11.6 \text{ ppm}$. Considering

this as a possible calibration errors and adding this error quadratically to the model error, we would obtain $\Delta\alpha/\alpha = -21.3 \pm 11.8$ ppm.

We also note that the Fe II and Si II lines shown in Fig. 7 have different profiles. The simultaneous presence of a strong C IV and low ionized ions supposes a complex ionization structure which may lead to the velocity shifts between different ions.

3.2 HE 0001–2340.

3.2.1 The $z_{\text{abs}} = 2.185$ system

The normalized spectra of Fe II and Mg II lines from the $z_{\text{abs}} = 2.185$ systems towards HE 0001–2340 are shown in Fig. 8. The $\lambda 2600$ and $\lambda 2586$ lines, not shown, are blended with strong telluric absorptions and are not considered. The signal-to-noise ratio per pixel at the continuum level is ~ 130 for the Fe II lines and ~ 80 for the Mg II lines. The corresponding pixel sizes (binning 2×2 pixels) at the positions of the Fe II and Mg II lines are of 2.4 km s^{-1} .

A simple 2-component model is sufficient to describe the observed profiles and the corresponding synthetic profiles are shown by the smooth lines in Fig. 8.

In this system we use only the $\lambda 2382$ line since the $\lambda 2344$ line is giving a very large velocity shift of 600 m s^{-1} (~ 0.4 pixel size) which we think anomalous (for details, see L07b). From the analysis of the Fe II $\lambda 1608$ and Fe II $\lambda 2382$ lines we obtain $\Delta\alpha/\alpha = 23.2 \pm 10.4$ ppm. As in the preceding system here again the $\Delta\alpha/\alpha$ value and its error suggest the presence of some hidden systematics.

The present system shows unsaturated Mg II lines with profiles similar to the Fe II lines and radial velocities of the doublet consistent within $|dv| \leq 100 \text{ m s}^{-1}$. In the MM method the Mg II lines are used as ‘anchors’ due to their low sensitivity to α variations. The system under study reveals much more homogeneous ionization structure as compared to the system described above and, hence, allows us to assume small Doppler shifts between lines of different ions, in particular between Fe II and Mg II. The synthetic profiles are shown in Fig. 8, right column. The $\Delta\alpha/\alpha$ value we derive comparing Mg II and Fe II is $\Delta\alpha/\alpha = 3.2 \pm 2.6$ ppm. However, we note that if an error accounting for the calibration uncertainty of the order of 11.6 ppm as derived before were added, then we would obtain $\Delta\alpha/\alpha = 3.2 \pm 18.1$ ppm.

3.2.2 The $z_{\text{abs}} = 2.187$ system

The Fe II lines in this system at $z_{\text{abs}} = 2.187$ shown in Fig. 9 are considerably stronger as compared to the previous system. The relative shift between the red Fe II lines and $\lambda 1608$ yields $\Delta\alpha/\alpha = 20.8 \pm 3.1$ ppm. At face value this result is providing a positive variation of $\Delta\alpha/\alpha$ with a C.L. of about 7σ but of opposite sign of what derived towards HE 1347–2457. Again we believe that also this result points to the presence of significant systematic errors probably due to the calibration. Including an estimate of the calibration uncertainty as before, we would have $\Delta\alpha/\alpha = 20.8 \pm 12.0$ ppm.

The comparison of the position of the Mg II and Fe II lines reveals something very peculiar. The fitting of the strongest Fe II $\lambda 2344$ and Mg II lines shows that the relative shift between them is extremely large and reaches 1.6 km s^{-1} . The shift is of almost 0.7 pixel size and can be even seen by eye in Fig. 9, right column. Taking this result at face value, it would give $\Delta\alpha/\alpha \sim -90$ ppm. This value is even larger than any conceivable calibration error and is suggesting something different.

The system shows a plenty of lines of ions in different ionization stages ranging from neutral species such as O I and C I to highly ionized such as C IV and O VI. This suggests that the observed velocity shift between Mg II and Fe II could be caused by the inhomogeneous ionization.

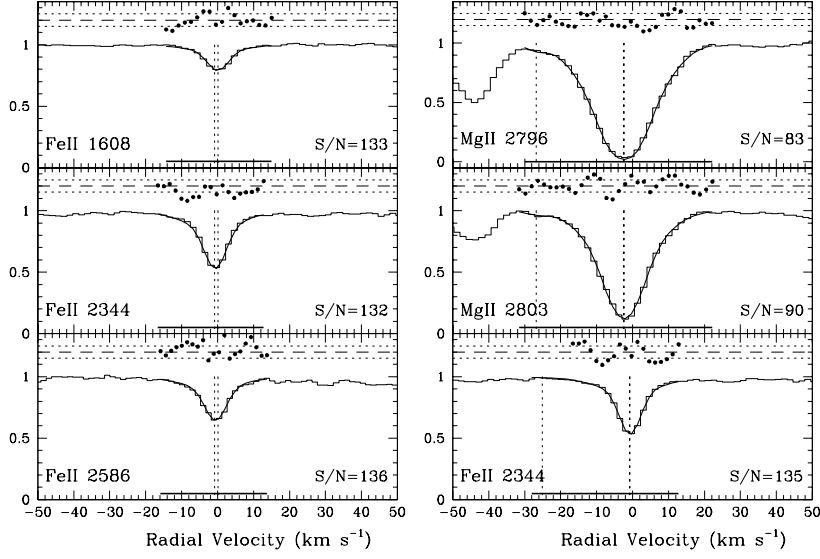


Fig. 9. Fe II and Mg II associated with the $z_{\text{abs}} = 2.187$ system towards HE 0001–2340. The zero radial velocity is fixed at $z = 2.187155$. The normalized χ^2_ν is equal to: 1.52 ($\nu = 50$) for the Fe II $\lambda\lambda 1608, 2344, 2586$ lines, and to 1.20 ($\nu = 76$) for the combined Mg II $\lambda\lambda 2796, 2803$ and Fe II $\lambda 2344$ lines.

Table 2. Comparison of results from CSPA, MWF06 and this paper ($\Delta\alpha/\alpha$ in units of 10^{-6})

QSO	z_{abs}	$\Delta\alpha/\alpha$ CSPA	$\Delta\alpha/\alpha$ MWF06*	$\Delta\alpha/\alpha$ this work**	χ^2_ν	lines used
(1)	(2)	(3)	(4)	(5)	(6)	(7)
1347–2457	1.493	0 ± 5	-12.7 ± 3.6	-21.3 ± 11.8	1.60	Fe II $\lambda\lambda 1608, 2344, 2586$. Fe II $\lambda\lambda 2344, 2586$; Si II $\lambda\lambda 1526, 1808$.
0001–2340	2.185			23.2 ± 15.6 3.2 ± 18.1	0.71 1.33	Fe II $\lambda\lambda 1608, 2382$. Fe II $\lambda 2382$; Mg II $\lambda\lambda 2796, 2803$. Fe II $\lambda\lambda 2344, 2382$; Mg II $\lambda\lambda 2796, 2803$; Si II $\lambda 1526$; Al II $\lambda 1670$.
	2.187	-2 ± 2	-12.2 ± 5.3	20.8 ± 12.0	1.46	Fe II $\lambda\lambda 1608, 2344, 2586$. Fe II $\lambda\lambda 2344, 2374, 2586$; Si II $\lambda 1526$; Al II $\lambda 1670$; Mg II $\lambda 2803$.

* The errors in Col. 4 are those given in Table 1 from MWF06 divided by their $\sqrt{\chi^2_\nu}$ values.

** The errors include a calibration error of 11.6 ppm, see text.

3.3 Results from the SIDAM analysis of the Chand et al. sample

The $\Delta\alpha/\alpha$ estimated of CSPA and our SIDAM measurements are summarized in Table 2 for comparison. The recent reanalysis of MWF06 of the CSPA data, obtained on base of Fe II, Mg II, Si II, and Al II lines, are also given in the Table.

Our analysis with the SIDAM methodology of the CSMP data suggests that the VLT/UVES spectra adopted by Chand et al. are affected by uncontrolled calibration errors mimicking $\Delta\alpha/\alpha$ at the level of 10s ppm. This is best illustrated by $\Delta\alpha/\alpha$ values derived from Fe II lines only, but this was already pointed out in L06 on the basis of Fig. 1(b) of CSPA. In this figure of CSPA the accuracy of wavelength calibration is checked through the relative velocity shifts between the Fe II $\lambda 2344$ and $\lambda 2600$ lines. With a good calibration the mean $\langle \Delta v \rangle$ should be consistent with zero since the sensitivity coefficients of the two Fe lines are very similar. On the

other hand the figure in the CSPA shows a significant dispersion of $\sigma_{\Delta v} \simeq 0.4 \text{ km s}^{-1}$. This scatter transforms into an error $\sigma_{\Delta\alpha/\alpha} \sim 20 \text{ ppm}$, which is even larger of what assumed here. Surprisingly, such errors do not show up in the Chand et al. results which gives a very small dispersion around zero values. Recently the same VLT/UVES spectra and the same absorption systems were re-analyzed by MWF06 who obtained significantly different values for $\Delta\alpha/\alpha$ and much larger errors for most of the systems. CSPA set a too low tolerance on the halting the calculations while deriving the $\chi^2(\Delta v)$ curves. As a consequence, the minima of these curves, i.e. the most probable values of $\Delta\alpha/\alpha$, and their confidence limits were not accurately estimated.

The new results for the systems investigated here are given in Table 2. The results of MWF06 seems to require also some intrinsic scatter or larger errors in agreement with our analysis based only on the Fe II lines. Our results are much in line with those of MWF06 with the notable difference of the system at $z_{\text{abs}} = 2.187$ towards HE 0001-2340 where we found results with opposite sign. This can be easily explained with the Doppler shift between Mg II and Fe II ions we detected in this system. As noted before this shift is driving $\Delta\alpha/\alpha$ towards large negative values and this is precisely what found by MWF06. The possibility of such shifts has important bearings on the MM method in general, which, to estimate $\Delta\alpha/\alpha$, uses lines of different ions. Such a possibility has been also discussed in some detail in Bahcall et al. (2004). Doppler shifts could be of random nature and would be canceled out if averaged over a large sample of measurements as in Murphy et al. (2003, hereafter MWF03). However, the uncertainties due to inhomogeneous ionization leading to Doppler shifts between different ions should be included in the total error budget of the individual $\Delta\alpha/\alpha$ measurements because these errors determine the weights and, thus, the values of the weighted mean and its uncertainty. A priori it is not possible to say whether the averaging over several $\Delta\alpha/\alpha$ values will deliver a true $\Delta\alpha/\alpha$ value. This motivated a study of the statistical properties of the whole $\Delta\alpha/\alpha$ sample from MWF03 given in L07b and which are briefly reported in the following chapter.

4 Statistical analysis of the Murphy et al. sample

The accuracy of the $\Delta\alpha/\alpha$ estimates obtained by statistical methods averaging over a large data array should be checked against systematic effects. In the approach by MWF03, the accuracy of a single $\Delta\alpha/\alpha$ measurement is of the order of 10 ppm (see Table 3), and only averaging over an hundred of individual $\Delta\alpha/\alpha$ values from different redshifts can provide an accuracy of the sample mean at 1 ppm level if the $1/\sqrt{n}$ -rule is applicable to the data in question.

The distribution of the MWF03 data shown in Fig. 10 reveals pronounced tails. In the sample there are also some measurements where the negative $\Delta\alpha/\alpha$ values of several tens of ppm with the significance $\geq 3\sigma$ are unlikely to be true. For instance the system at $z_{\text{abs}} = 2.8433$ towards QSO 1946+7658 has a $\Delta\alpha/\alpha = -47.4 \pm 12.9 \text{ ppm}$. Other notable cases are the data points No. 12, 17 and 25 in Table 3. Since the size of the sample is large enough, it would be wise to flag these systems or remove them from statistical calculations. The quadratically added estimate of the unweighted variance is 278.9 ppm^2 , whereas the variance of the individual data points is 552.2 ppm^2 suggesting that the variance of the MWF03 sample may be underestimated. Indeed, peculiar clustering is noticeable in Table 3 where several systems show very close $\Delta\alpha/\alpha$ values (points 37-41, 52, 54, 55, 57, or 78-81).

A simple but nevertheless effective way to obtain a robust estimate is the β -trimmed mean where $\beta\%$ data points are removed from each side of the distribution (Hampel et al. 1986). Assuming a standard 5% for β , we obtain a robust 5%-trimmed mean of $-3.9 \pm 1.5 \text{ ppm}$ weighted and $-3.7 \pm 1.7 \text{ ppm}$ unweighted.

Another check is to see whether the data points belonging to different subsamples are identically distributed. The total sample can be divided into two groups according to the data with or without Mg II lines. The means of both subsamples are $\Delta\alpha/\alpha = -4.8 \pm 1.2 \text{ ppm}$ and $-1.1 \pm 1.7 \text{ ppm}$ more than 2σ apart. We note that all the signal is carried by the first subsample which shows negative $\Delta\alpha/\alpha$ at 4σ confidence level while the second one yields a result consistent with zero.

The error of the mean decays with the sample size n as \sqrt{n} only for independent, i.e. non-correlated, data. Any violation of independency leads to the underestimation of the error, which

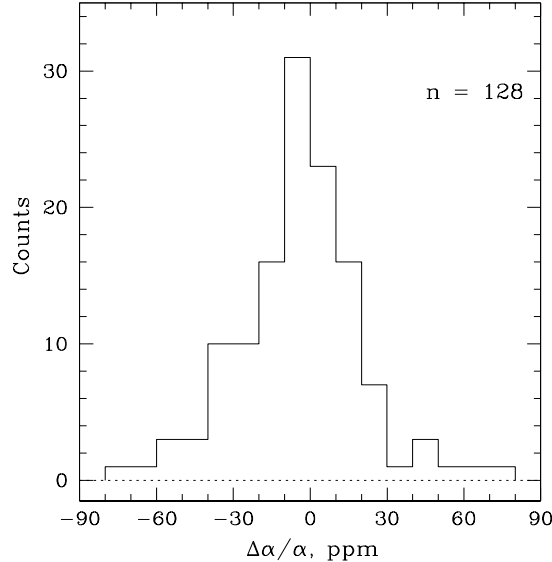


Fig. 10. Histogram of the MWF03 sample from Table 3.

becomes especially significant for the large size samples. It should be noted that practically all series of physical measurements are somewhat correlated (e.g., Mosteller & Tukey 1977; Elyasberg 1984; Hampel et al. 1986; Künsch et al. 1993; Hampel 2000). Since the MWF03 sample is quite large, it is possible to check the behavior of the error of the weighted mean as a function of the sample size with the statistical procedure described in Chap. 8 in Hampel et al. (1986). From the total sample we form p groups with n elements randomly selected. The sample size of $n_{\text{total}} = 128$ allows $4 \leq p \leq 12$ groups with $30 \geq n \geq 10$ points in each. For every group we calculate the weighted mean and then from p values of the mean we can calculate its variance and standard deviation, σ_m (the error of the mean). In this way we obtain the dependence of σ_m on the group size. For independent variables this error goes as $1/\sqrt{n}$, but if the data are correlated, then the error decays slower and has a non-zero limit at $n \rightarrow \infty$.

The error σ_m as a function of the group size n is shown in Fig. 11 by open squares for the ‘raw’ MWF03 sample. The function $n^{-0.5}$ is plotted by the dashed line. It is seen that the error of the weighted mean decreases more slowly than that for the independent data: in the range $10 < n < 30$ the calculated points can be approximated by the curve $n^{-0.425}$ (the smooth line in Fig. 11). This implies that the real error of the mean is at least 1.5 times larger than that estimated on base of the $1/\sqrt{n}$ -rule.

5 ESPRESSO time

ESPRESSO stems for Echelle Spectrograph for PREcision Super Stable Observation and is a new instrument proposed by a consortium of European institutes for the incoherent combined focus of the VLT array (Pasquini, 2008). It provides a resolving power of $R = 45000$ collecting the light from the 4 VLT units, as an equivalent 16 m telescope, or of $R = 180000$ for 1 VLT unit, while incorporating many of the innovative solutions of the HARPS spectrograph specialized in hunting exoplanets by means of radial velocity variations. Thus, ESPRESSO will provide more photons, more resolution and more stability with the promise to improve by at least one order of magnitude the accuracy of the $\Delta\alpha/\alpha$ measurements by means of QSO absorption lines (Molaro, 2008). Thus a definitive solution of the case for a variability of $\Delta\alpha/\alpha$ at the level of ~ 0.1 ppm will be within reach.

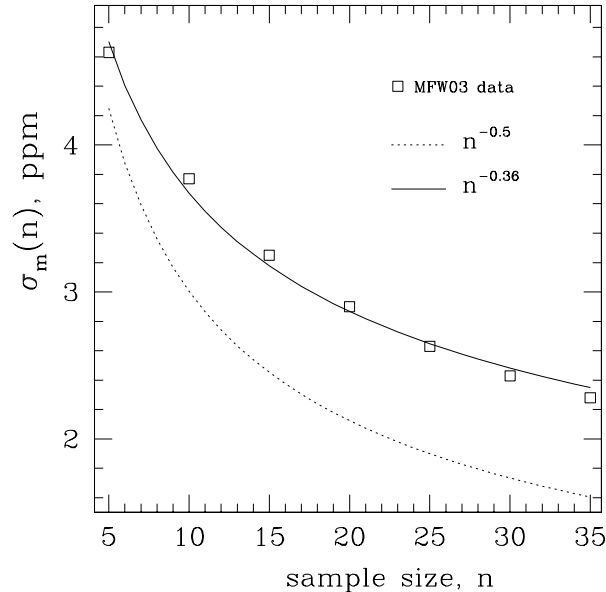


Fig. 11. The error of the weighted mean σ_m for the total MFW03 dataset (squares) as a function of the sample size n . The real error of the mean decays slower than $n^{-0.5}$ expected for independent data (see text for detail).

6 Conclusions

In this study we have presented the SIDAM methodology for deriving $\Delta\alpha/\alpha$ by means of the Fe II lines observed in the intervening systems in QSO spectra. We have analyzed 3 sets of data used to derive constraints on a hypothetical dependence of the fine-structure constant α on cosmic time: (a) we have revised our previous estimate of $\Delta\alpha/\alpha$ in the $z_{\text{abs}} = 1.15$ system from L06 obtained with the VLT/UVES, (b) we have analyzed with SIDAM method three absorption systems included in the sample of CSPA, and (c) considered the statistical properties of the sample of MFW03 obtained from Keck/HIRES spectra of QSOs. The main results and conclusions are as follows.

1. The estimates of $\Delta\alpha/\alpha$ are at $z_{\text{abs}} = 1.15$ towards HE 0515–4414 and at $z_{\text{abs}} = 1.84$ towards Q 1101–264 providing $\Delta\alpha/\alpha = -0.12 \pm 1.79$ ppm and $\Delta\alpha/\alpha = 5.66 \pm 2.67$ ppm, respectively, are the most accurate currently estimates of $\Delta\alpha/\alpha$. A potential systematic uncertainty which can affect these values is a relative shift of the wavelength scales in the blue and red arms of the UVES where the distant Fe lines are recorded simultaneously. However, Molaro et al. (2007) by means of asteroid observations able to control small shifts at the level of $\approx 30 \text{ m s}^{-1}$ revealed no significant radial velocity shifts between the two UVES arms.
2. To test the CSPA results we analyzed from their sample three absorption systems identified in the spectra of HE 1347–2457 and HE 0001–2340, where the $\Delta\alpha/\alpha$ can be measured by means of Fe II lines only. The systems contain the Fe II $\lambda\lambda 1608, 2344, 2382, 2586$ and 2600 \AA lines which allows us to estimate $\Delta\alpha/\alpha$ free from uncertainties related to the inhomogeneous ionization. The pipeline-reduced VLT/UVES spectra used in CSPA show relative radial velocity shifts between the Fe II lines mimicking the variability of α at the level of 10s ppm. There are no easy ways to evaluate the statistical properties of these calibration errors and therefore the CSPA data are not suitable for the $\Delta\alpha/\alpha$ estimates at the ppm level.
3. The statistical analysis of the MFW03 sample shows some correlations in the dataset previously overlooked setting a limit on the achievable accuracy of the weighted mean from the applicability of the σ/\sqrt{n} -rule. A robust estimate of $\Delta\alpha/\alpha$ from a 5%-trimmed MFW03

sample is $\Delta\alpha/\alpha = -3.9 \pm 1.5$ ppm (weighted) or $\Delta\alpha/\alpha = -3.7 \pm 1.7$ ppm (unweighted), but it is not clear whether the errors of the individual measurements are still underestimated.

Acknowledgements. This research is supported by the DFG project RE 353/48-1, the RFBR grant No. 06-02-16489, the FASI grant NSh 9879.2006.2.

References

1. Aldenius, M., Johansson, S., & Murphy, M. T., MNRAS **370** (2006) 444–452
2. Ashenfelter, T., Mathews, G. J., & Olive, K. A., Phys. Rev. Lett. **92**, (2004) 041102-1–4
3. Avelino, P. P., Martins, C. J. A. P., Nunes, N. J., & Olive, K. A., Phys. Rev. D **74**, (2006) 083508-1–7
4. Bahcall, J. N., Steinhardt, C. L., & Schlegel, D., ApJ **600**, (2004) 520–543
5. Chand, H., Srianand, R., Petitjean, P., Aracil, B., Quast, R., & Reimers, D., A&A **451**, (2006) 45–56
6. Chand, H., Srianand, R., Petitjean, P., & Aracil, B., A&A **417**, (2004) 853–871 [CSPA]
7. Coc A., Nunes, N.J., Olive, K. A., Uzan, J.P., Vangioni, E. 2007, Phys. rev. D **76**, (2007) 3511
8. Dent, T., Stern, S., & Wetterich, C., J. Phys. G Special Issue, in press, (2007) arXiv: astro-ph/0710.4854
9. Dzuba, V. A., Flambaum, V. V., Kozlov, M. G., & Marchenko, M. V., Phys. Rev. A **66**, (2002) 022501-1–8
10. Dzuba, V. A., Flambaum, V. V., & Webb, J. K., Phys. Rev. Lett. **82**, (1999) 888–891
11. de Cuyper, J.-P., & Hensberge, H., A&AS **129**, (1998) 409–416
12. Elyasberg, P. E., Cosmic Research **22**, (1984) 643–650
13. Fujii, Y., Phys. Lett. B **616**, (2005) 141–144
14. Fujii, Y., eprint, (2007) arXiv: astro-ph/0709.2211
15. Gould, C. R., Sharapov E. I., & Lamoreaux, S. K., Phys. Rev. C **74**, (2006) 024607-1–10
16. Hampel, F., Research Report No. **93**, (2000) (Seminar für Statistik, Eidgenössische Technische Hochschuler, <http://ftp.stat.math.ethz.ch/Research-Reports/>)
17. Hampel, F. R., Ronchetti, E. M., Rousseeuw P. J., & Stahel W. A., *Robust Statistics. The Approach Based on Influence Functions* (John Wiley & Sons, N.Y., 1986)
18. Hao, H., Stanek, K. Z., Dobrzycki, A. et al., ApJ **659**, (2007) L99–L102
19. Kaufer, A., D’Odorico, S., & Kaper, L., *UV-Visual Echelle Spectrograph. User Manual*, (2004) (<http://www.eso.org/instruments/uves/userman/>)
20. Kozlov, M. G., Korol, V. A., Berengut, J. C., Dzuba, V. A., & Flambaum, V. V., Phys. Rev. A **70**, (2004) 062108-1–6
21. Künsch, H., Beran, J., & Hampel, F., Ann. Statist. **21**, (1993) 943–964
22. Levshakov, S. A., Molaro, P., Lopez, S. et al., A&A **466**, (2007a) 1077–1082 [L07a]
23. Levshakov, S. A., Agafonova, I. I., Molaro, P., & Reimers, D., A&A submitted, (2007b) [L07b]
24. Levshakov, S. A., Centurión, M., Molaro, P., et al., A&A **449**, (2006) 879–889
25. Levshakov, S. A., Centurión, M., Molaro, P., & D’Odorico, S. A&A **434**, (2005) 827–838
26. Levshakov, S. A., 2004, in *Astrophysics, Clocks and Fundamental Constants*, eds. S. G. Karshenboim and E. Peik (Springer-Verlag, Berlin, 2004) 151–166
27. Levshakov, S. A., MNRAS **269**, (1994) 339–348
28. Marciano, W. J., Phys. Rev. Lett. **52**, (1984) 489–491
29. Martins, C. J. A. P., in *Precision Spectroscopy in Astrophysics*, eds. L. Pasquini, M. Romaniello and N. C. Santos (Springer-Verlag, Berlin, 2007) in press, arXiv: astro-ph/0610665
30. Molaro, P., ASS Proceedings *Science with the VLT in the ELT Era* (ed. A. Moorwood 2008)
31. Molaro, P., Levshakov, S. A., Monai, S. Centurión, M., Bonifacio, P., D’Odorico S., & Monaco, L., A&A in press, astro-ph/ 07123345 (2007)
32. Morton, D. C., ApJS **149**, (2003) 205–238
33. Mosteller, F., & Tukey, J. W., *Data Analysis and Regression* (Addison-Wesley, Reading, MA, 1977)
34. Mota, D. F., & Barrow, J. D., MNRAS **349**, (2004) 291–302
35. Murphy, M. T., Webb, J. K., & Flambaum, V. V., eprint, (2006) arXiv: astro-ph/0612407 [MWF06]
36. Murphy, M. T., Flambaum, V. V., Webb, J. K., et al. in *Astrophysics, Clocks and Fundamental Constants*, eds. S. G. Karshenboim and E. Peik (Springer-Verlag, Berlin, 2004), 131–150
37. Murphy, M. T., Webb, J. K., & Flambaum, V. V., MNRAS **345**, (2003) 609–638 [MWF03]

38. Palmer, B. A., & Engleman, R., Jr., *Atlas of the Thorium Spectrum* (Los Alamos National Laboratory, Los Alamos, 1983)
39. Pasquini, L., ASS Proceedings *Science with the VLT in the ELT Era* (ed. A. Moorwood, 2008)
40. Peik, E., Lipphardt, B., Schnatz, H., et al. 2006, arXiv: physics/0611088
41. Porsev, S. G., Koshelev, K. V., Tupitsyn, I. I., Kozlov, M. G., Reimers, D., & Levshakov, S. A., Phys. Rev. A in press, (2007) arXiv: physics.atom-ph/0708.1662
42. Quast, R., Reimers, D., & Levshakov, S. A., A&A **415**, (2004) L7–L11
43. Varshalovich, D. A., & Levshakov, S. A., JETP Lett. **58**, (1993) 237–240
44. Webb, J. K., Flambaum, V. V., Churchill, C. W., Drinkwater, M. J., & Barrow, J. D., Phys. Rev. Lett. **82**, (1999) 884–887

Table 3. $\Delta\alpha/\alpha$ with associated 1σ statistical error from Keck/HIRES QSO absorption spectra (MWF03). A symbol ‘*’ in Cols. 1 and 6 indicates systems with Mg II lines.

No.	Object	z_{abs}	$\Delta\alpha/\alpha$ (ppm)	$\sigma_{\Delta\alpha/\alpha}$ (ppm)	No.	Object	z_{abs}	$\Delta\alpha/\alpha$ (ppm)	$\sigma_{\Delta\alpha/\alpha}$ (ppm)
1	0000 – 2620	3.3897	-76.66	32.31	65	0002 + 0507	0.85118	-3.46	12.79
*2	1244 + 3142	0.85048	-68.97	70.12	*66	2206 – 1958	1.0172	-3.22	7.32
*3	1009 + 2956	1.1117	-54.61	25.18	*67	1206 + 4557	0.92741	-2.75	7.76
4	2230 + 0232	1.8585	-54.07	23.40	*68	0117 + 2118	1.0479	-2.23	22.00
5	0149 + 3335	2.1408	-51.12	29.76	*69	1206 + 4557	0.92741	-2.18	13.89
6	1946 + 7658	2.8433	-47.43	12.89	70	1946 + 7658	1.7385	-2.12	18.57
7	0841 + 1256	2.4761	-43.04	28.54	71	0237 – 2321	1.3650	-1.97	5.65
8	2233 + 1310	3.1513	-40.05	33.01	*72	0302 – 2223	1.0092	-1.89	10.08
9	0100 + 1300	2.3095	-39.41	24.98	73	1549 + 1919	1.1425	-0.76	6.71
10	0201 + 3634	2.4563	-37.31	22.85	74	2359 – 0216	2.0951	-0.68	22.11
*11	2206 – 1958	0.94841	-36.59	18.55	*75	1248 + 4007	0.85452	-0.21	12.68
*12	0841 + 1256	1.0981	-35.89	12.03	*76	2344 + 1228	1.1161	0.09	19.63
*13	1254 + 0443	0.51934	-33.71	32.47	77	0216 + 0803	1.7680	0.44	12.35
14	2231 – 0015	2.6532	-33.48	28.27	*78	1222 + 2251	0.66802	0.67	14.74
15	2344 + 1228	2.5378	-32.05	20.94	*79	0117 + 2118	0.72913	0.84	12.97
*16	0002 + 0507	0.59137	-31.00	24.28	*80	2145 + 0643	0.79026	0.87	5.89
*17	0450 – 1312	1.1743	-30.70	10.98	*81	1421 + 3305	0.84324	0.99	8.47
18	1549 + 1919	1.8024	-30.50	24.73	*82	1437 + 3007	1.2259	3.08	14.60
*19	1421 + 3305	1.1726	-28.44	14.48	*83	0058 + 0155	0.61256	3.74	11.89
20	0347 – 3819	3.0247	-27.95	34.29	*84	0454 + 0356	0.85929	4.05	13.25
*21	0055 – 2659	1.3192	-26.42	24.57	85	1425 + 6039	2.8268	4.33	8.27
*22	0058 + 0155	0.72508	-26.37	35.22	86	2343 + 1232	1.5899	4.53	11.87
23	2231 – 0015	2.0653	-26.04	23.23	*87	0002 + 0507	0.85118	4.94	10.21
*24	1634 + 7037	0.99010	-21.94	13.43	88	1223 + 1753	2.5577	5.46	11.99
*25	0153 + 7427	0.74550	-21.68	7.78	*89	0841 + 1256	1.1314	5.62	7.87
26	0956 + 1217	2.3103	-21.61	59.77	90	0201 + 3634	2.4628	5.72	27.06
*27	1107 + 4847	1.0158	-20.86	9.34	*91	1317 + 2743	0.66004	5.90	15.15
*28	1107 + 4847	0.86182	-20.30	16.32	*92	0117 + 2118	1.3246	6.95	8.03
*29	1626 + 6433	0.58596	-19.77	45.29	93	0201 + 3634	2.3240	7.58	15.92
*30	1148 + 3842	0.55339	-18.61	17.16	*94	0528 – 2505	0.94398	7.59	23.35
31	1850 + 4015	1.9900	-16.63	22.60	95	0741 + 4741	3.0173	7.94	17.96
*32	0450 – 1312	1.2294	-14.72	8.36	96	0528 – 2505	2.8114	8.50	22.55
*33	1202 – 0725	1.7549	-14.65	21.82	97	0930 + 2858	3.2351	8.67	17.77
34	0757 + 5218	2.6021	-13.96	19.55	98	0019 – 1522	3.4388	9.25	39.58
*35	0636 + 6801	1.2938	-13.92	6.23	*99	0450 – 1312	1.2324	10.17	27.52
*36	0055 – 2659	1.5337	-13.19	10.72	*100	1634 + 7037	0.99010	10.94	24.59
*37	0741 + 4741	1.6112	-12.99	17.26	*101	1107 + 4847	0.80757	11.99	12.22
*38	1225 + 3145	1.7954	-12.96	10.49	*102	2231 – 0015	1.2128	12.23	14.65
*39	0117 + 2118	1.3428	-12.90	9.48	103	2348 – 1444	2.2794	13.46	41.80
*40	1213 – 0017	1.5541	-12.68	8.92	104	1225 + 3145	1.7954	13.52	13.88
*41	0000 – 2620	1.4342	-12.56	11.67	*105	2206 – 1958	1.0172	13.54	8.83
42	2343 + 1232	2.4300	-12.24	21.26	106	2206 – 1958	2.0762	14.29	30.22
*43	0449 – 1325	1.2667	-12.12	14.30	107	0841 + 1256	2.3742	14.35	24.24
*44	2343 + 1232	0.73117	-12.11	9.75	*108	1254 + 0443	0.93426	14.85	19.08
*45	1421 + 3305	0.90301	-9.98	17.83	109	1223 + 1753	2.4653	16.35	19.19
46	2230 + 0232	1.8640	-9.98	21.47	*110	0055 – 2659	1.2679	16.69	27.45
47	2343 + 1232	2.1711	-9.61	12.95	111	2231 – 0015	2.0653	17.07	24.35
*48	1011 + 4315	1.4162	-8.92	5.52	112	2233 + 1310	2.5548	17.32	63.49
49	1442 + 2931	2.4389	-8.82	14.73	113	2206 – 1958	1.9204	18.78	22.05
50	0528 – 2505	2.1406	-8.53	22.68	114	0201 + 3634	1.9550	19.89	23.38
51	1759 + 7539	2.6253	-7.50	25.08	*115	1248 + 4007	0.77292	21.65	11.91
*52	0454 + 0356	1.1534	-7.49	17.82	116	0841 + 1256	2.3742	22.77	43.51
53	0207 + 0503	3.6663	-7.48	34.68	117	1244 + 3142	2.7504	24.14	41.10
*54	2344 + 1228	1.0465	-7.47	15.30	118	1011 + 4315	2.9587	24.75	26.98
*55	1549 + 1919	1.3422	-7.40	12.32	*119	1307 + 4617	0.22909	25.51	53.92
56	0241 – 0146	2.0994	-7.39	26.75	120	1055 + 4611	3.3172	27.06	56.77
*57	1213 – 0017	1.3196	-7.38	7.60	121	2233 + 1310	2.5480	29.42	52.07
58	1626 + 6433	2.1102	-7.05	10.68	122	0757 + 5218	2.8677	38.37	32.88
59	1425 + 6039	2.7698	-6.88	18.43	123	1337 + 1121	2.7955	41.03	85.38
*60	0201 + 3634	1.4761	-6.47	12.19	*124	0420 – 0127	0.63308	42.11	40.76
*61	0841 + 1256	1.2189	-5.22	5.42	125	2359 – 0216	2.1539	43.46	33.38
62	1759 + 7539	2.6253	-4.92	26.60	126	1215 + 3322	1.9990	56.48	37.64
*63	0940 – 1050	1.0598	-4.53	15.72	127	1132 + 2243	2.1053	63.23	36.22
*64	0823 – 2220	0.91059	-3.94	6.09	*128	0119 – 0437	0.65741	71.23	45.99